

# GS-I<sup>3</sup>: Gaussian Splatting for Surface Reconstruction from Illumination-Inconsistent Images

Tengfei Wang, Yongmao Hou, Zhaoning Zhang, Yiwei Xu, Zongqian Zhan and Xin Wang

**Abstract**—Accurate geometric surface reconstruction, providing essential environmental information for navigation and manipulation tasks, is critical for enabling robotic self-exploration and interaction. Recently, 3D Gaussian Splatting (3DGS) has gained significant attention in the field of surface reconstruction due to its impressive geometric quality and computational efficiency. While recent relevant advancements in novel view synthesis under inconsistent illumination using 3DGS have shown promise, the challenge of robust surface reconstruction under such conditions is still being explored. To address this challenge, we propose a method called GS-I<sup>3</sup>. Specifically, to mitigate 3D Gaussian optimization bias caused by underexposed regions in single-view images, based on Convolutional Neural Network (CNN), a tone mapping correction framework is introduced. Furthermore, inconsistent lighting across multi-view images, resulting from variations in camera settings and complex scene illumination, often leads to geometric constraint mismatches and deviations in the reconstructed surface. To overcome this, we propose a normal compensation mechanism that integrates reference normals extracted from single-view image with normals computed from multi-view observations to effectively constrain geometric inconsistencies. Extensive experimental evaluations demonstrate that GS-I<sup>3</sup> can achieve robust and accurate surface reconstruction across complex illumination scenarios, highlighting its effectiveness and versatility in this critical challenge. <https://github.com/TFwang-9527/GS-3I>

## I. INTRODUCTION

Accurate geometric surface reconstruction is a fundamental support for robotic self-exploration and interaction, providing crucial 3D environmental information for tasks such as navigation, manipulation, decision-making, etc. [1], [2]. As robots increasingly operate in unstructured and complex environments, the ability to perform surface reconstruction with high precision, robustness, and adaptability becomes increasingly critical. Traditional methods for surface reconstruction often rely on multi-view stereo (MVS) techniques or depth sensors[3], [4], which, while effective in controlled conditions, typically involve complex computational steps and are time-consuming, thus limiting their applicability in practice.

In contrast, recent advancements in 3D Gaussian Splatting (3DGS)[5] have introduced a promising approach to surface reconstruction. Until now, 3DGS has attracted significant

attention due to its superior geometric quality and computational efficiency, positioning it as a promising candidate for real-time applications in challenging environments[6], [7]. Its capability to produce high-quality surface representations marks a notable improvement over traditional techniques[16].

However, despite these advances, 3DGS still faces significant challenges when dealing with inconsistent illumination, a common issue in real-world scenarios[14], [15]. Although 3DGS has demonstrated considerable success in novel view synthesis under such conditions[11], [13], [12], the task of achieving robust and accurate surface reconstruction remains unresolved. Inconsistent lighting can introduce 3D Gaussian optimization biases, disrupt geometric constraints, and lead to deviations in the reconstructed surface. These challenges ultimately compromise the accuracy, fidelity, and reliability of the surface reconstruction, hindering its practical application in complex environments where lighting conditions are highly variable.

To address these challenges, we propose a novel method called GS-I<sup>3</sup>. Our approach is designed to mitigate the adverse effects of inconsistent illumination on surface reconstruction by introducing two key innovations: a tone mapping correction framework based on CNN and a normal compensation mechanism that integrates reference normals extracted from single-view images with normals computed from multi-view observations.

The first contribution, tone mapping correction framework, is designed to address the optimization bias caused by underexposed regions in single-view images. Underexposed regions often contain insufficient texture and detail, leading to inaccurate depth estimates and surface reconstructions as shown in Fig.1. By leveraging an CNN-based tone mapping correction, our method can adaptively adjust the exposure levels of these regions, ensuring that the optimization process is not biased towards overexposed or underexposed areas. This correction framework enhances the overall quality of the reconstructed surface by providing more reliable images for the reconstruction process.

The second contribution, normal compensation mechanism, tackles the problem of geometric constraint mismatches caused by inconsistencies in lighting across multi-view images. Variations in camera settings and complex scene illumination can lead to significant differences in the appearance of the same scene across different views, resulting in mismatches in the geometric constraints used for reconstruction, as shown in Fig.1. To overcome this, our method integrates reference normals extracted from single-view images with normals computed from multi-view obser-

\*This work was supported by the National Natural Science Foundation of China (No.42301507) and Natural Science Foundation of Hubei Province, China (No. 2022CFB727).

<sup>1</sup>Tengfei Wang, Yongmao Hou, Zhaoning Zhang, Yiwei Xu, Zongqian Zhan, Xin Wang are with the School of Geodesy and Geomatics, Wuhan University, China PR. (Corresponding Author: Xin Wang, xwang@sgg.whu.edu.cn)

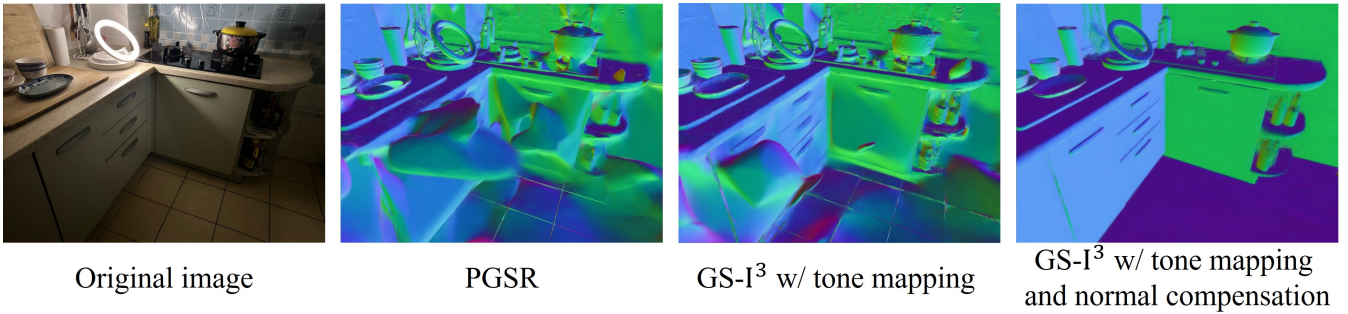


Fig. 1. Original image on the Kitchen data(subset of Gaussian in the dark dataset), along with the normal maps obtained by the different methods.

vations. This integration allows for a more robust and accurate estimation of surface normals, effectively constraining geometric inconsistencies and improving the overall quality of the reconstructed surface.

Extensive experimental evaluations demonstrate the efficacy of our GS-I<sup>3</sup> in achieving robust and accurate surface reconstruction across complex illumination scenarios. Our method outperforms existing approaches in terms of geometric accuracy, highlighting its potential for real-world applications in robotic exploration and interaction.

## II. RELATED WORK

In this section, two related topics are reviewed including surface reconstruction and inconsistent illumination processing

### A. Surface Reconstruction

Traditional surface reconstruction methods have largely relied on multi-view stereo (MVS) pipelines, which triangulate correspondences across images to infer depth and geometry. These approaches, such as COLMAP[16] and PMVS[17], excel in structured environments with consistent lighting but struggle with textureless regions, occlusions, and computational inefficiency in large-scale scenes. To address these limitations, sensor fusion techniques integrating LiDAR, RGB-D cameras, or structured light have been proposed, offering higher accuracy at the cost of hardware complexity and limited scalability[18].

The advent of neural implicit representations, particularly Neural Radiance Fields (NeRF)[19], revolutionized the field by enabling high-fidelity scene modeling through differentiable volume rendering. Subsequent works extended NeRF for surface reconstruction by incorporating signed distance functions (SDFs) or occupancy networks, achieving impressive results in both geometry and appearance[20], [21]. However, these methods remain computationally intensive and sensitive to illumination variations due to their reliance on photometric consistency.

In recent years, 3D Gaussian Splatting (3DGS) has emerged as a groundbreaking approach by integrating explicit geometric primitives with differentiable rasterization techniques, enabling real-time rendering with remarkable efficiency. This method represents scenes using anisotropic 3D Gaussians, achieving state-of-the-art performance in both

reconstruction quality and computational efficiency[7], [9], making it particularly suitable for real-time interactive applications such as robotics. Extensions of 3DGS, including dynamic scene surface reconstruction [22] and semantic-aware surface reconstruction[23], further demonstrate the versatility of this framework. While 3DGS has shown significant potential in the field of surface reconstruction, existing methods have limited exploration in addressing surface reconstruction under challenging conditions with significant illumination variations and inconsistent lighting. This research gap motivates our work to adapt 3DGS for illumination-robust geometric modeling, aiming to tackle the challenges posed by complex lighting environments.

### B. Inconsistent Illumination Processing

Inconsistent lighting poses a fundamental challenge to multi-view reconstruction as it violates the brightness constancy assumption that most multi-view methods rely on[27]. Early solutions primarily focused on correcting the photometric properties of input views, such as adjusting image brightness and contrast using methods like histogram equalization[28]. Although these methods have shown promising results in laboratory settings, their applicability and practicality are significantly limited for robotic systems operating in complex, uncontrolled environments.

In the realm of NeRF-based 3D reconstruction methods, researchers have proposed various solutions. HDR-NeRF[24] and Raw-NeRF[25] have successfully recovered normally lit scenes from inconsistently lit images by utilizing HDR and RAW format data. However, the stringent requirements for input data make these methods difficult to apply directly to RGB data commonly captured by robots. NeRF-W[26] attempts to directly process RGB images in wild environments by modeling lighting variations as appearance embeddings, which to some extent mitigates the artifacts in rendering. Nevertheless, the lengthy computation time of this method severely limits its application in robotic exploration tasks that require high real-time performance.

In recent years, 3DGS technology has demonstrated significant advantages in the field of 3D reconstruction due to its fast and efficient rendering capabilities. In response to the rendering challenges under inconsistent lighting conditions, new methods based on 3DGS have emerged.

Vastgaussian[14] decouples the appearance of scenes under complex lighting and applies mapping transformations to rendered images to adapt to appearance changes; LO-Gaussian[10] innovatively introduces the concept of a simulated filter between real and rendered images, recovering scenes from overexposed and overly dark lighting by simulating the degradation process; Dark in the Gaussian[11] approaches from the perspective of exposure, designing a camera response module to compensate for lighting inconsistencies in multi-view scenarios. However, these methods primarily optimize for rendering tasks, and a systematic solution for surface reconstruction in inconsistently lit scenes remains lacking, which is a critical issue that current research urgently needs to address.

### III. METHOD

In the task of surface reconstruction under inconsistent illumination conditions, two critical challenges are predominantly encountered: 3D Gaussian optimization bias induced by exposure variation within a single view, and inconsistency in Geometry caused by illumination variations across multiple views. To address these limitations, this study proposes a novel surface reconstruction method, termed GS-I<sup>3</sup>, specifically designed for scenes with inconsistent illumination. The proposed method comprises two pivotal components: Firstly, in Section III-A, we introduce an adaptive tone mapping framework based on CNN, which effectively balances illumination inconsistencies within a single view. Secondly, in Section III-B, we devise a normal compensation mechanism that utilizes pre-trained normal maps from single views to rectify reconstruction errors arising from illumination-inconsistent images. The workflow is shown in Fig.2.

#### A. Adaptive Tone Mapping Framework

In the proposed adaptive tone mapping framework, a Convolutional Neural Network (CNN) is employed to dynamically adjust the brightness and contrast of an image based on its local pixel context. The framework ensures that low-exposure (dark) regions are enhanced while preventing overexposure in bright areas. The CNN extracts local features, such as edges, textures, and shapes, through a series of convolutional layers. These features enable the network to identify regions requiring significant adjustments (e.g., underexposed areas) while leaving well-exposed regions largely unchanged.

The CNN architecture consists of two convolutional layers followed by two fully connected layers. The first convolutional layer (conv1) extracts low-level features, while the second convolutional layer (conv2) captures higher-level features. The output of the convolutional layers is flattened and passed through two fully connected layers (fc1 and fc2), which predict the per-pixel parameters  $\alpha$  (gain factor) and  $\gamma$  (gamma correction factor). Specifically, the fc2 layer outputs a 2-dimensional vector for each pixel, where the first dimension corresponds to  $\gamma$  and the second dimension corresponds to  $\alpha$ .

The model predicts two key parameters for each pixel in the image:  $\alpha$  (gain factor) and  $\gamma$  (gamma correction factor). These parameters are used to adaptively modify pixel brightness and contrast, ensuring that dark regions are brightened and details are revealed, while overexposure is avoided. The brightness of each pixel  $p_i$  is mapped to a new value  $p'_i$  using the following transformation:

$$p'_i = \alpha_i \cdot p_i^{\gamma_i} \quad (1)$$

where  $\alpha_i$  and  $\gamma_i$  are the gain and gamma correction factors predicted by the CNN for pixel  $i$ . This transformation is applied to each pixel individually, allowing for localized adjustments that adapt to the image’s content.

The CNN is trained to learn these mappings through a loss function designed to optimize two primary objectives: (1) enhancing contrast in dark regions and (2) preventing overexposure in bright regions. The loss function is composed of the following components:

**Dark Region Enhancement Loss:** To enhance contrast in dark regions, the model encourages smaller gamma values ( $\gamma_i$ ) for pixels with low brightness. This is achieved by penalizing the average gamma value in dark regions, defined as pixels with brightness below a threshold (e.g.,  $p_i < 0.3$ ). The dark region enhancement loss is computed as:

$$L_{\text{dark}} = -\frac{1}{n_d} \sum_{i \in \text{dark}} \gamma_i \quad (2)$$

where  $n_d$  is the number of pixels in the dark region. By minimizing this loss, the model learns to brighten and enhance contrast in underexposed areas.

**Overexposure Prevention Loss:** To prevent overexposure, the model penalizes pixels with brightness values exceeding a predefined threshold (e.g.,  $p'_i > 0.9$ ). The overexposure loss is computed as:

$$L_{\text{over}} = \frac{1}{n_o} \sum_{i \in \text{over}} (p'_i - 0.9)^2 \quad (3)$$

where  $n_o$  is the number of overexposed pixels. This loss ensures that the model avoids excessive brightness adjustments that could lead to loss of detail in bright regions.

The total loss function combines these components with appropriate weighting factors:

$$L_{\text{tone}} = \lambda_{\text{dark}} \cdot L_{\text{dark}} + \lambda_{\text{over}} \cdot L_{\text{over}} \quad (4)$$

where  $\lambda_{\text{dark}}$  and  $\lambda_{\text{over}}$  are hyperparameters controlling the relative importance of each objective.

During training, the CNN iteratively updates its parameters  $\theta$  to minimize the total loss. This optimization process ensures that the model learns to adaptively adjust brightness and contrast based on the local pixel context. After training, the model applies the learned  $\alpha$  and  $\gamma$  parameters to each pixel, resulting in an image where dark regions are brightened and details are enhanced, while overexposure is avoided in bright regions.

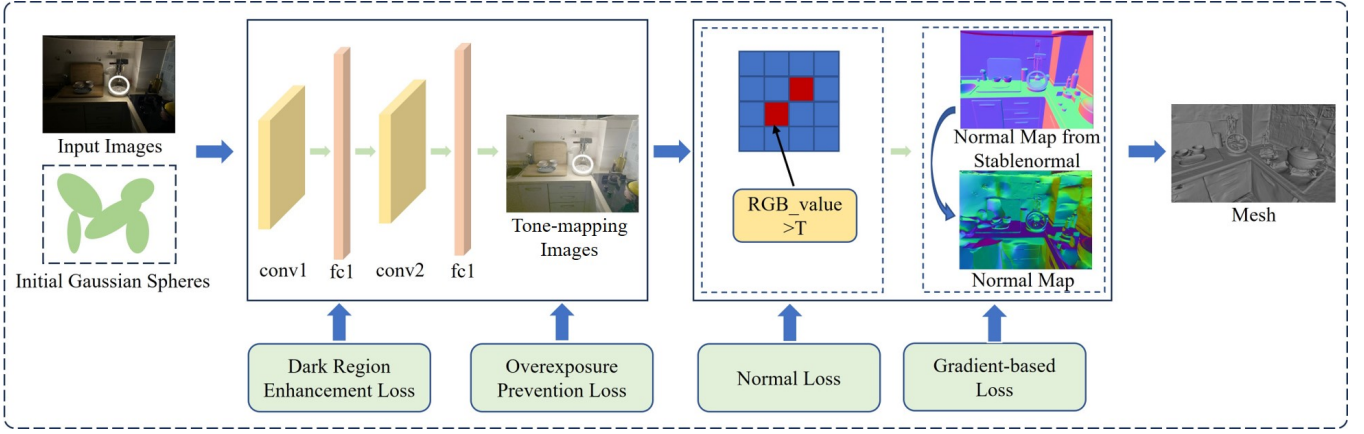


Fig. 2. The workflow of GS-I<sup>3</sup>.

### B. Normal Compensation

The Adaptive Tone Mapping Framework can map the brightness of a single view to an appropriate range. However, illumination inconsistencies between different views can lead to significant fluctuations in Gaussian spheres, thereby reducing the accuracy of surface reconstruction. Building on the single-view adaptive tone mapping method, we devise a normal compensation mechanism that utilizes pre-trained normal maps from single views to rectify reconstruction errors arising from illumination-inconsistent images.

First, during the training process, we identify pixels requiring correction using a combined RGB loss  $L_{\text{RGB}}$ . The RGB loss is defined as a weighted sum of the SSIM and L1 losses between the rendered pixels and the ground truth pixels, with weights of 0.2 and 0.8, respectively:

$$L_{\text{RGB}}(i) = 0.2 \cdot L_{\text{SSIM}}(i) + 0.8 \cdot L_1(i), \quad (5)$$

where  $L_{\text{SSIM}}(i)$  is the structural similarity loss for the  $i$ -th pixel, and  $L_1(i)$  is the pixel-wise L1 loss. We set a threshold  $T$  to determine whether a pixel requires correction. For pixels with  $L_{\text{RGB}}(i) > T$ , we compute a normal loss based on the difference between the predicted normals and the normals generated by a pre-trained large model, such as StableNormal [29]. Trained on a large dataset, StableNormal provides robust normal predictions that capture fine geometric details. This normal loss is used to guide the correction of the predicted normals during training.

For pixels with  $L_{\text{RGB}}(i) > T$ , the normal loss is defined as the L1 difference between the predicted normals and the normals generated by the StableNormal model. The normal loss for the  $i$ -th pixel is given by:

$$L_{\text{normal}}(i) = \begin{cases} 0 & \text{if } L_{\text{RGB}}(i) \leq T, \\ \|N_i^{\text{pred}} - N_i^{\text{StableNormal}}\|_1 & \text{if } L_{\text{RGB}}(i) > T, \end{cases} \quad (6)$$

where  $N_i^{\text{pred}}$  is the originally predicted normal, and  $N_i^{\text{StableNormal}}$  is the normal predicted by StableNormal.

However, merely correcting the normals is insufficient for accurate surface reconstruction, as it only adjusts the

normal directions without ensuring local consistency. To address this, we introduce a gradient-based loss term  $L_{\text{gradient}}$  that penalizes discrepancies between the gradients of the predicted normals and the gradients of the normals generated by StableNormal. This term encourages smooth and locally consistent normal fields, which are essential for high-quality surface reconstruction:

$$L_{\text{gradient}} = \sum_{i=1}^n \left\| \nabla N_i^{\text{pred}} - \nabla N_i^{\text{StableNormal}} \right\|_1, \quad (7)$$

where  $\nabla N_i^{\text{pred}}$  and  $\nabla N_i^{\text{StableNormal}}$  are the spatial gradients of the predicted normals and the normals generated by StableNormal, respectively. This term ensures that the predicted normals exhibit smooth and locally consistent variations, which are critical for accurate surface reconstruction.

The final loss function combines SSIM loss, L1 loss, normal compensation loss, gradient-based normal consistency loss, and tone mapping loss, and is expressed as:

$$L_{\text{total}} = \lambda_1 L_{\text{SSIM}} + \lambda_2 L_1 + \lambda_3 L_{\text{normal}} + \lambda_4 L_{\text{gradient}} + \lambda_5 L_{\text{tone}}, \quad (8)$$

where  $\lambda_1, \lambda_2, \lambda_3, \lambda_4, \lambda_5$  are hyperparameters used to balance the weights of different loss terms. Here,  $L_{\text{SSIM}}$  measures structural similarity,  $L_1$  quantifies pixel-wise brightness errors,  $L_{\text{normal}}$  corrects normals for high-loss pixels,  $L_{\text{gradient}}$  enforces local consistency in the normal field, and  $L_{\text{tone}}$  represents the tone mapping loss.

## IV. EXPERIMENTS

### A. Experimental Setup

**Datasets and Metrics** To validate the effectiveness of our proposed method, GS-I<sup>3</sup>, in scenarios with inconsistent illumination, we utilized the illumination-inconsistent dataset introduced by Gaussian in the Dark [11]. This dataset comprises 12 real-world scenes (5 indoor and 7 outdoor), each containing approximately 80 to 130 naturally exposed images captured from multiple angles, with a resolution of 3991 × 2960. While this dataset is suitable for qualitative evaluation, it lacks ground truth for quantitative assessment. To address

this limitation, we introduced a modified version of the DTU dataset[30], a widely used benchmark with ground truth, by adding random lighting perturbations to simulate inconsistent illumination conditions. This modified DTU dataset enables qualitative evaluation of our method. Sample images are illustrated in the accompanying Fig.3.

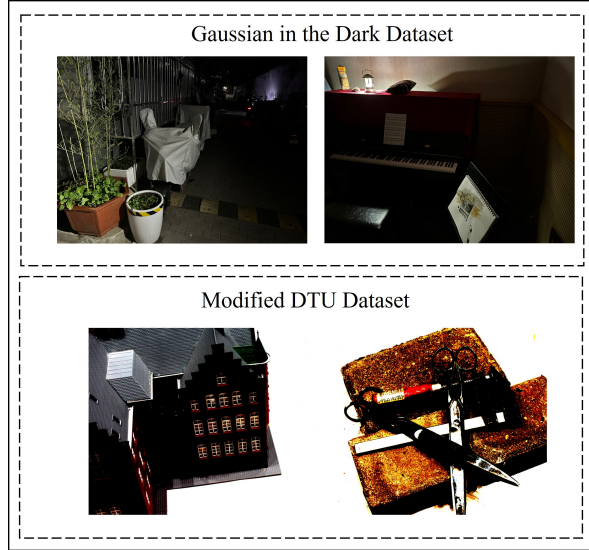


Fig. 3. Sample images of Gaussian in the Dark dataset and Modified DTU dataset.

**Baselines and Implementation.** To the best of our knowledge, our method is the first to tackle surface reconstruction using illumination-inconsistent images, there are no directly comparable baseline methods available. To evaluate the effectiveness of GS-I<sup>3</sup>, we compared it with three state-of-the-art surface reconstruction methods: PGSR[9], 2DGS[7], GOF[8] and SuGaR[6], which are the most relevant ones to our work.

### B. Comparison with SOTA Methods

Fig.4 and Fig.5 present a qualitative comparison of the proposed GS-I<sup>3</sup> method with other existing methods (PGSR, 2DGS, GOF, and SuGaR) in scenarios with inconsistent lighting conditions on modified DTU dataset and Dark in the Gaussian dataset. It is clearly observed that GS-I<sup>3</sup> generates surface models that more accurately reflect the actual scene, whereas other methods exhibit significant reconstruction errors. These errors mainly manifest as surface geometry distortion, holes, and unrealistic geometric structures.

The primary cause of these errors lies in the inconsistent lighting across images captured from different angles in such scenes. The varying exposure results in considerable brightness differences for the same scene area across different images. These brightness discrepancies make it challenging for previous gaussian-based methods based on multi-view geometric constraints to accurately fit the true surface geometry during the training process. Specifically, conventional 3DGS-based methods rely heavily on Gaussian splatting distribution to model the scene surface. However, due to lighting inconsistencies, Gaussian splatting attempts

to satisfy rendering requirements from different viewpoints during optimization, leading to erroneous distributions in the air. While these erroneous distributions can reduce discrepancies between viewpoints during rendering, they significantly deviate from the actual surface geometry, causing a notable decline in reconstruction quality.

In contrast, GS-I<sup>3</sup> addresses this issue with two key contributions. First, at the single-view level, GS-I<sup>3</sup> introduces an adaptive tone mapping framework based on CNN, effectively balancing the lighting inconsistencies within a single image. Specifically, the method enhances the contrast of dark regions while preserving the details of bright areas, thereby strengthening the loss constraint in dark regions during training, which significantly improves the reconstruction quality of dark areas. Second, at the multi-view level, GS-I<sup>3</sup> employs a normal compensation mechanism, leveraging pre-trained single-view normals to correct lighting inconsistencies across multiple views. This mechanism introduces pre-trained normal information, eliminating the lighting ambiguity for the same region across different views, thus providing a more accurate representation of the surface geometry.

The comparison results in Fig.4 and 5 demonstrate that GS-I<sup>3</sup> is capable of reconstructing surface models with rich details and accurate geometry under complex lighting conditions, while other methods show noticeable distortions and errors in highlights, shadows, and dark areas. This outcome strongly validates the superiority of GS-I<sup>3</sup> in scenes with inconsistent lighting.

Tab.I presents the quantitative comparison of the proposed method with other methods on the modified DTU dataset. The experiments cover multiple scenes, each involving varying degrees of lighting changes. The Chamfer Distance metric is employed for geometric accuracy evaluation, as it comprehensively reflects the geometric deviation between the reconstructed surface and the true surface.

As shown in the results in Tab.I, GS-I<sup>3</sup> outperforms all other methods in every scene of the DTU dataset, achieving significantly lower chamfer distance values. This result is consistent with the qualitative analysis in 5 and further confirms the effectiveness of GS-I<sup>3</sup> in scenarios with inconsistent lighting. Additionally, due to the low accuracy of mesh obtained by some methods, which makes it impossible to complete ICP(Iterative Closest Point) registration with the ground truth point cloud for evaluation of chamfer distance, we aligned the ground truth point cloud to the mesh obtained by COLMAP[16] under original lighting conditions to complete the accuracy assessment. This approach ensures a fair and consistent evaluation across all methods.

### C. Ablation Study

To validate the effectiveness of the individual components in the GS-I<sup>3</sup> method, we conducted ablation experiments on the modified DTU dataset, focusing on scan37 and scan114, as well as the Gaussian in the Dark dataset, focusing on the Kitchen and Living room subset. These experiments were designed to evaluate the contribution of each individual component to the overall performance. Specifically,

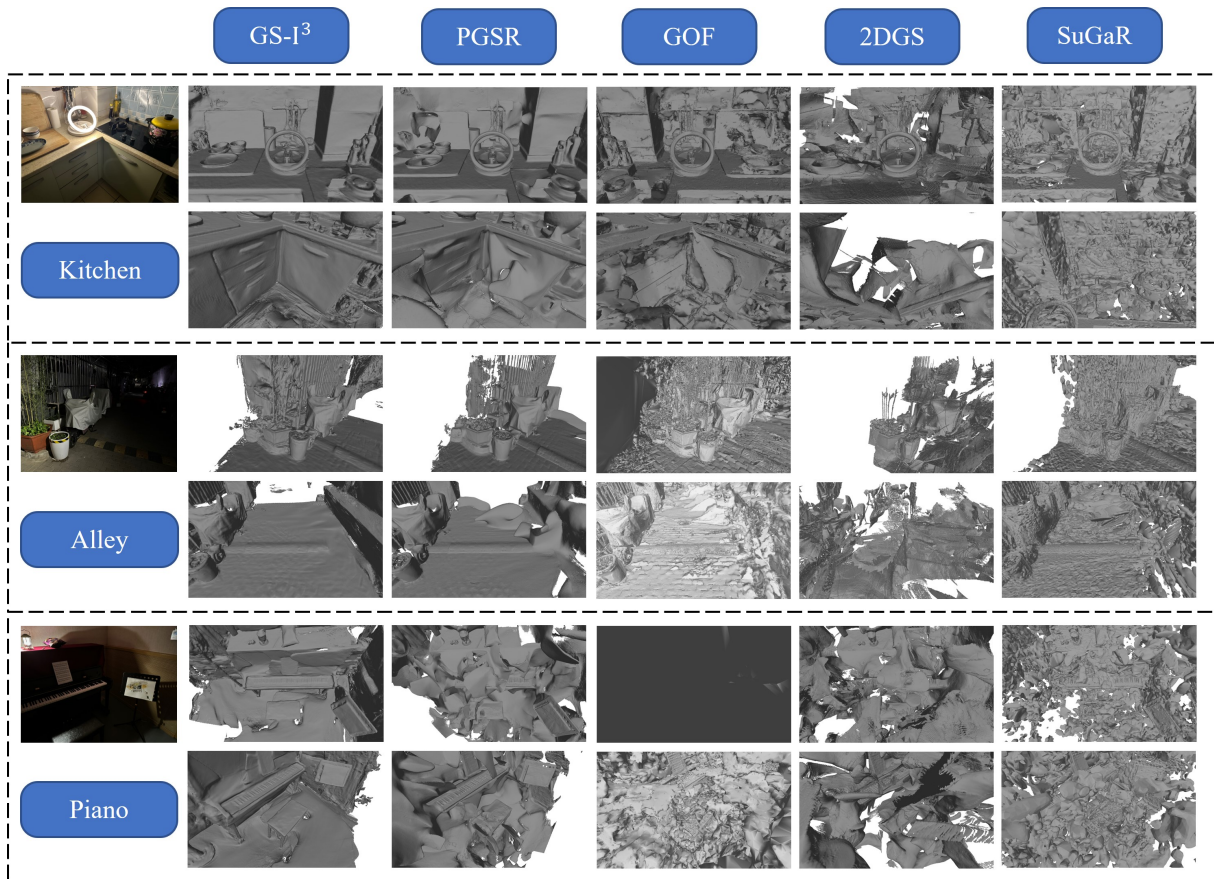


Fig. 4. Comparison of mesh reconstruction results across the Gaussian in the Dark dataset with various methods.

TABLE I

COMPARISON OF DIFFERENT METHODS ON THE MODIFIED DTU DATASET. WHERE THE FIRST LINE IS THE NUMBER OF DIFFERENT DATA IN THE DATASET, AND THE CHAMFER DISTANCE UNIT IS CENTIMETERS(LOWER VALUES INDICATE BETTER PERFORMANCE)

Method	24	37	40	55	63	65	69	83	97	105	106	110	114	118	122	Mean
SuGaR	4.14	2.96	1.66	1.29	4.63	2.97	1.99	3.83	2.14	3.63	2.88	1.86	3.19	4.92	2.58	2.98
2DGS	3.71	3.24	2.01	1.76	3.70	2.34	2.40	4.11	3.66	2.40	2.80	3.46	2.88	3.08	4.29	2.90
GOF	4.45	3.01	2.43	2.18	3.60	1.52	2.61	3.28	0.88	1.70	2.39	2.33	1.30	1.77	1.47	2.26
PGSR	3.09	1.50	2.05	1.13	2.02	0.98	2.74	3.14	1.65	0.84	1.79	1.57	1.16	2.07	0.71	1.76
<b>GS-I<sup>3</sup></b>	<b>2.81</b>	<b>0.81</b>	<b>0.91</b>	<b>1.07</b>	<b>1.72</b>	<b>0.78</b>	<b>0.63</b>	<b>2.42</b>	<b>0.63</b>	<b>0.71</b>	<b>0.54</b>	<b>0.88</b>	<b>0.50</b>	<b>1.10</b>	<b>0.37</b>	<b>1.07</b>

we performed the following experiments: (1) using only the adaptive tone mapping framework, (2) using only the normal compensation, and (3) disabling both the adaptive tone mapping framework and the normal compensation. The qualitative results of these ablation experiments are shown in Fig.6, while the quantitative results are presented in Tab.II.

TABLE II

COMPARISON OF DIFFERENT METHODS IN THE ABLATION STUDY ON THE MODIFIED DTU DATASET (SELECTED SCANS).

Method	scan37	scan114
(1)	1.34	0.98
(2)	1.12	0.77
(3)	1.50	1.16
<b>GS-I<sup>3</sup></b>	<b>0.81</b>	<b>0.50</b>

From the quantitative results in Tab.II, the experimental re-

sults clearly demonstrate that using only the normal compensation has the most significant impact on the completeness and accuracy of the scene reconstruction. When only the pre-trained normal constraint is applied, the reconstruction quality is notably improved, especially under complex lighting conditions. From the qualitative results in Fig.6, it is evident that the normal compensation corrects the direction of normals that are erroneous due to inconsistent lighting. This component effectively resolves lighting ambiguities across multiple views, enabling a more precise representation of surface geometry. It addresses issues caused by inconsistent lighting, such as surface distortion and unrealistic geometric structures.

On the other hand, as shown in Tab.II and Fig.6, when only the single-view tone mapping equilibrium is applied, the results indicate that this method still enhances the overall

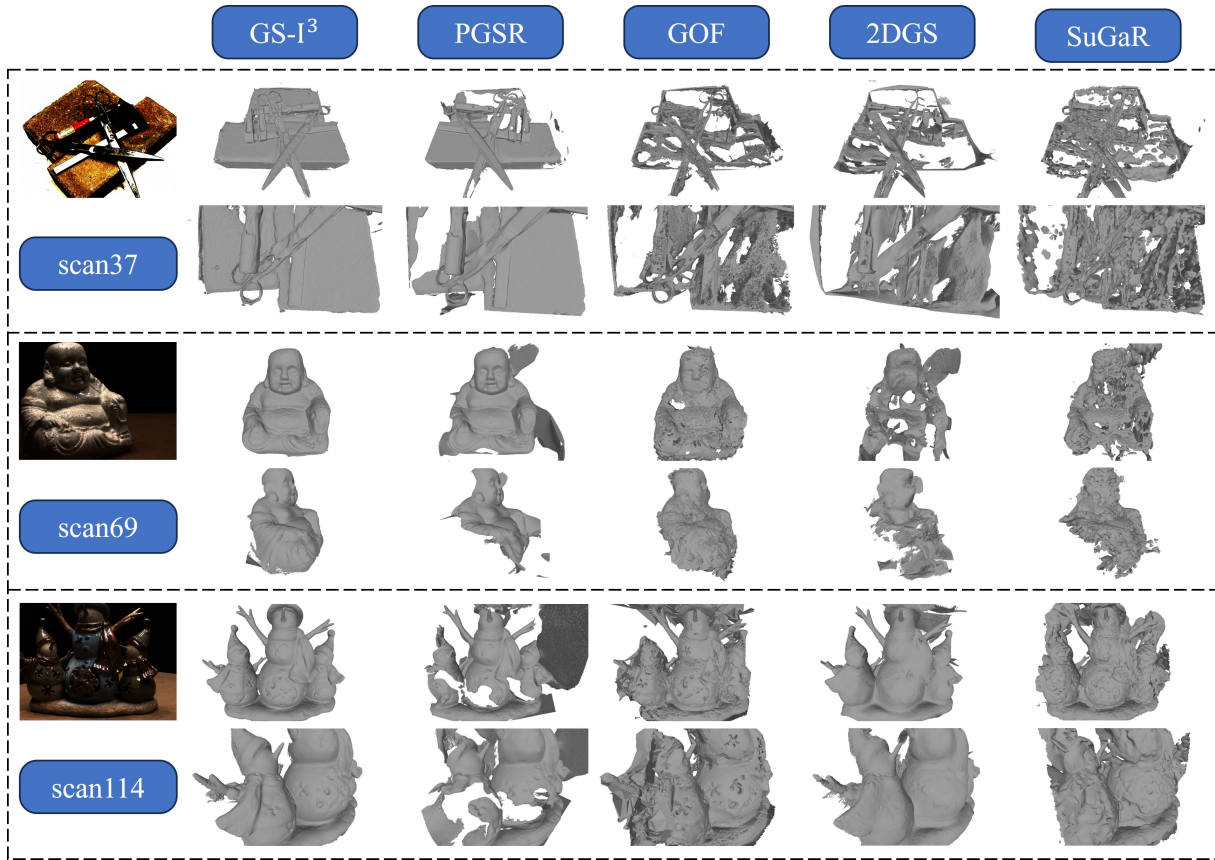


Fig. 5. Comparison of mesh reconstruction results across the modified DTU dataset with various methods.

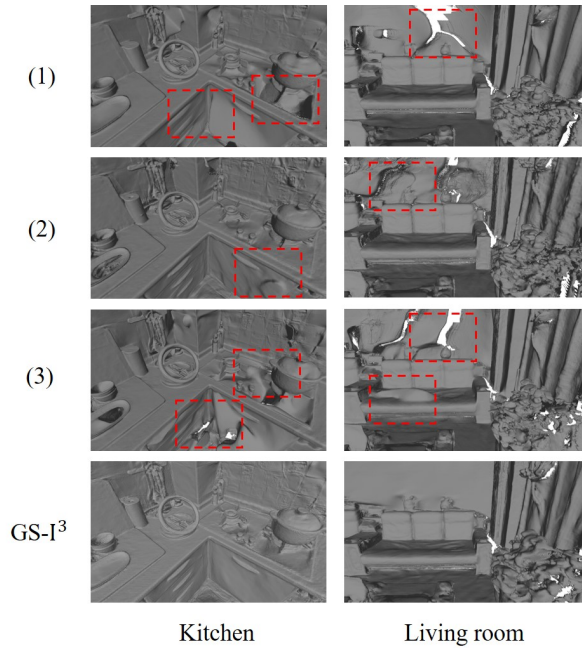


Fig. 6. Comparison of different methods in the ablation study on the modified Gaussian in the dark dataset (selected scenes).



Fig. 7. Comparison of different methods in the ablation study on the modified Gaussian in the dark dataset (selected scenes).

reconstruction quality to some extent, particularly in handling lighting variations within individual images. This component helps to increase contrast in darker regions while preserving details in brighter areas, thereby improving the representation of surface features in these regions. As shown in Fig.7, the overall brightness and contrast of the tone-mapping image

are significantly enhanced, and the objects in the image become much clearer.

From both the quantitative and qualitative results, when the two components are combined, the best reconstruction results are achieved. Furthermore the tone-mapping images allow the pre-trained model to predict the actual normals more accurately, reducing ambiguities caused by dark or overexposed regions. Therefore, our method leverages the synergy between these components to achieve optimal performance.

## V. CONCLUSION AND LIMITATION

In this paper, we present GS-I<sup>3</sup>, a novel method for accurate surface reconstruction using inconsistent illumination images. By addressing critical challenges such as exposure variation within single-view images and geometric inconsistencies across multiple views, our GS-I<sup>3</sup> effectively reconstructs complex surfaces in challenging lighting environments. The integration of an CNN-based adaptive tone mapping framework and a normal compensation mechanism enables the system to adapt to complex illumination, improving both surface detail and accuracy. Extensive experimental results demonstrate the superiority of GS-I<sup>3</sup> over existing 3DGS-based methods, particularly in terms of reducing geometric deviations and improving overall reconstruction quality. Furthermore, ablation studies confirm the efficacy of each individual component. Robustness of GS-I<sup>3</sup> in handling lighting inconsistencies across diverse environments highlights its potential for applications in robotic exploration and 3D surface reconstruction under real-world conditions.

## REFERENCES

- [1] J. Wang, Z. Gong, B. Tao, and Z. Yin, "A 3-d reconstruction method for large freeform surfaces based on mobile robotic measurement and global optimization," *IEEE Transactions on Instrumentation and Measurement*, vol. 71, pp. 1–9, 2022.
- [2] S. Lee, L. Chen, J. Wang, A. Liniger, S. Kumar, and F. Yu, "Uncertainty guided policy for active robotic 3d reconstruction using neural radiance fields," *IEEE Robotics and Automation Letters*, vol. 7, no. 4, pp. 12 070–12 077, 2022.
- [3] E. K. Stathopoulou and F. Remondino, "A survey on conventional and learning-based methods for multi-view stereo," *The Photogrammetric Record*, vol. 38, no. 183, pp. 374–407, 2023.
- [4] S. M. Seitz, B. Curless, J. Diebel, D. Scharstein, and R. Szeliski, "A comparison and evaluation of multi-view stereo reconstruction algorithms," in *2006 IEEE computer society conference on computer vision and pattern recognition (CVPR'06)*, vol. 1. IEEE, 2006, pp. 519–528.
- [5] B. Kerbl, G. Kopanas, T. Leimkühler, and G. Drettakis, "3d gaussian splatting for real-time radiance field rendering," *ACM Trans. Graph.*, vol. 42, no. 4, pp. 139–1, 2023.
- [6] A. Guédon and V. Lepetit, "Sugar: Surface-aligned gaussian splatting for efficient 3d mesh reconstruction and high-quality mesh rendering," in *Proceedings of the IEEE/CVF Conference on Computer Vision and Pattern Recognition*, 2024, pp. 5354–5363.
- [7] B. Huang, Z. Yu, A. Chen, A. Geiger, and S. Gao, "2d gaussian splatting for geometrically accurate radiance fields," in *ACM SIGGRAPH 2024 conference papers*, 2024, pp. 1–11.
- [8] Z. Yu, T. Sattler, and A. Geiger, "Gaussian opacity fields: Efficient and compact surface reconstruction in unbounded scenes," *arXiv preprint arXiv:2404.10772*, 2024.
- [9] D. Chen, H. Li, W. Ye, Y. Wang, W. Xie, S. Zhai, N. Wang, H. Liu, H. Bao, and G. Zhang, "Pgsr: Planar-based gaussian splatting for efficient and high-fidelity surface reconstruction," *arXiv preprint arXiv:2406.06521*, 2024.
- [10] J. You, Y. Zhang, T. Zhou, Y. Zhao, and L. Yao, "Lo-gaussian: Gaussian splatting for low-light and overexposure scenes through simulated filter," 2024.
- [11] S. Ye, Z.-H. Dong, Y. Hu, Y.-H. Wen, and Y.-J. Liu, "Gaussian in the dark: Real-time view synthesis from inconsistent dark images using gaussian splatting," in *Computer Graphics Forum*, vol. 43, no. 7. Wiley Online Library, 2024, p. e15213.
- [12] S. Singh, A. Garg, and K. Mitra, "Hdrsplat: Gaussian splatting for high dynamic range 3d scene reconstruction from raw images," *arXiv preprint arXiv:2407.16503*, 2024.
- [13] Y. Cai, Z. Xiao, Y. Liang, M. Qin, Y. Zhang, X. Yang, Y. Liu, and A. Yuille, "Hdr-gs: Efficient high dynamic range novel view synthesis at 1000x speed via gaussian splatting," *arXiv preprint arXiv:2405.15125*, 2024.
- [14] J. Lin, Z. Li, X. Tang, J. Liu, S. Liu, J. Liu, Y. Lu, X. Wu, S. Xu, Y. Yan, *et al.*, "Vastgaussian: Vast 3d gaussians for large scene reconstruction," in *Proceedings of the IEEE/CVF Conference on Computer Vision and Pattern Recognition*, 2024, pp. 5166–5175.
- [15] T. Zhang, K. Huang, W. Zhi, and M. Johnson-Roberson, "Darkgs: Learning neural illumination and 3d gaussians relighting for robotic exploration in the dark," *arXiv preprint arXiv:2403.10814*, 2024.
- [16] J. L. Schonberger and J.-M. Frahm, "Structure-from-motion revisited," in *Proceedings of the IEEE conference on computer vision and pattern recognition*, 2016, pp. 4104–4113.
- [17] Y. Furukawa and J. Ponce, "Accurate, dense, and robust multiview stereopsis," *IEEE transactions on pattern analysis and machine intelligence*, vol. 32, no. 8, pp. 1362–1376, 2009.
- [18] Z. Li, P. C. Gogia, and M. Kaess, "Dense surface reconstruction from monocular vision and lidar," in *2019 International Conference on Robotics and Automation (ICRA)*. IEEE, 2019, pp. 6905–6911.
- [19] B. Mildenhall, P. P. Srinivasan, M. Tancik, J. T. Barron, R. Ramamoorthi, and R. Ng, "Nerf: Representing scenes as neural radiance fields for view synthesis," *Communications of the ACM*, vol. 65, no. 1, pp. 99–106, 2021.
- [20] P. Wang, L. Liu, Y. Liu, C. Theobalt, T. Komura, and W. Wang, "Neus: Learning neural implicit surfaces by volume rendering for multi-view reconstruction," *arXiv preprint arXiv:2106.10689*, 2021.
- [21] L. Yariv, J. Gu, Y. Kasten, and Y. Lipman, "Volume rendering of neural implicit surfaces," *Advances in Neural Information Processing Systems*, vol. 34, pp. 4805–4815, 2021.
- [22] W. Cai, W. Ye, P. Ye, T. He, and T. Chen, "Dynamurfgs: Dynamic surface reconstruction with planar-based gaussian splatting," *arXiv preprint arXiv:2408.13972*, 2024.
- [23] T. Wang, X. Wang, Y. Hou, Y. Xu, W. Zhang, and Z. Zhan, "Pg-sag: Parallel gaussian splatting for fine-grained large-scale urban buildings reconstruction via semantic-aware grouping," *arXiv preprint arXiv:2501.01677*, 2025.
- [24] X. Huang, Q. Zhang, Y. Feng, H. Li, X. Wang, and Q. Wang, "Hdrnerf: High dynamic range neural radiance fields," in *Proceedings of the IEEE/CVF Conference on Computer Vision and Pattern Recognition*, 2022, pp. 18 398–18 408.
- [25] B. Mildenhall, P. Hedman, R. Martin-Brualla, P. P. Srinivasan, and J. T. Barron, "Nerf in the dark: High dynamic range view synthesis from noisy raw images," in *Proceedings of the IEEE/CVF conference on computer vision and pattern recognition*, 2022, pp. 16 190–16 199.
- [26] R. Martin-Brualla, N. Radwan, M. S. Sajjadi, J. T. Barron, A. Dosovitskiy, and D. Duckworth, "Nerf in the wild: Neural radiance fields for unconstrained photo collections," in *Proceedings of the IEEE/CVF conference on computer vision and pattern recognition*, 2021, pp. 7210–7219.
- [27] T. Wang and V. J. Gan, "Enhancing 3d reconstruction of textureless indoor scenes with indoreal multi-view stereo (mvs)," *Automation in Construction*, vol. 166, p. 105600, 2024.
- [28] T. Celik and T. Tjahjadi, "Contextual and variational contrast enhancement," *IEEE Transactions on Image Processing*, vol. 20, no. 12, pp. 3431–3441, 2011.
- [29] C. Ye, L. Qiu, X. Gu, Q. Zuo, Y. Wu, Z. Dong, L. Bo, Y. Xiu, and X. Han, "Stablenormal: Reducing diffusion variance for stable and sharp normal," *ACM Transactions on Graphics (TOG)*, vol. 43, no. 6, pp. 1–18, 2024.
- [30] R. Jensen, A. Dahl, G. Vogiatzis, E. Tola, and H. Aanæs, "Large scale multi-view stereopsis evaluation," in *2014 IEEE Conference on Computer Vision and Pattern Recognition*. IEEE, 2014, pp. 406–413.